Inorg. Chem. **2004**, *43*, 6188–6194

Metal–Metal Bonding in $ScTaN_2$. A New Compound in the System ScN–TaN

R. Niewa,* D. A. Zherebtsov, W. Schnelle, and F. R. Wagner

Max-Planck-Institut für Chemische Physik fester Stoffe, Nöthnitzer Str. 40, 01187 Dresden, Germany

Received February 19, 2004

Gray microcrystalline powders of $ScTaN_2$ were prepared from solid-state reactions of δ-ScN with Ta_3N_5 powders at $T = 1770$ K. According to thermal analyses the compound is stable against oxidation by O_2 up to temperatures of $T = 800$ K. In an Ar atmosphere $ScTaN_2$ decomposes above $T = 1250$ K and in a N_2 atmosphere above $T = 2000$ K under release of N_2 to form δ-ScN and β-Ta_2N. The crystal structure (space group $P6_3/mmc$, No. 194, $a = 305.34(3)$ pm, $c = 1056.85(9)$ pm, $Z = 2$) was refined on the basis of X-ray and neutron powder diffraction data. It comprises alternating layers of $ScN_{6/3}$ octahedra and trigonal $TaN_{6/3}$ prisms, which are also observed in the binary nitrides δ-ScN and ϑ-TaN, respectively. A small degree of anti-site defects (about 5%) was detected. Only a small solubility of ScN in ϵ-TaN was observed, while the solubility of TaN in δ-ScN is $\geq$10 mol % at $T = 1820$ K. $ScTaN_2$ is a diamagnetic small gap semiconductor or a semimetal, as inferred from magnetization and electrical resistivity measurements, consistent with band structure calculations. Chemical bonding analyses with the COHP method yield significant covalent Ta–Ta interactions. Topological analyses of the electron localization function reveal unexpected Ta–Ta three-center bonding basins within seemingly empty trigonal prisms of the $TaN_{6/3}$ layers.

Introduction

For ternary tantalum-rich nitrides layered crystal structures have been described frequently. Typically, with Li and Mg either disordered rock-salt-type structures were obtained (e.g., $Li_2Ta_3N_5$, $Li_{2-x}Ta_{2+x}N_4$ and $Mg_{(8/3)-x}Ta_{(4/3)+x}N_4$),[1,2] or the crystal structures were discussed in terms of octahedrally coordinated Li^+, Mg^{2+}, and Ta^{5+}, while Ta^{3+} is predominately coordinated trigonally prismatically by N (e.g., in $Li_{1-x}Ta_{3+x}N_4$ and $Mg_{1-x}Ta_{2+x}N_3$).[2] The crystal structures of these phases are closely related to the crystal chemistry of the binary tantalum nitrides. With sodium and calcium the layered compounds $Na[TaN_2]$[3] and $Ca[TaN_2]$[4] were described to crystallize in the α-$NaFeO_2$ structure type with alternating layers of octahedrally coordinated Ta and Na or Ca, respectively, in a ternary ordered rock-salt-type variant. By shifting the layers of octahedra surrounding Ta, the delafossite structure type with linearly coordinated Cu^+ is obtained in $Cu[TaN_2]$.[5] Compounds $R_3[Ta_2N_6]$ with layers of all-basal corner-sharing quadratic pyramids $^2_\infty[TaN_{4/2}N^{4.5-}]$ form with rare-earth metals R = La, Ce, and Pr.[6] The reduced and nitrogen-deficient phase $ScTaN_{1-x}$ with a layered metal atom arrangement and nitrogen in octahedral interstices leads us to the nitride chemistry of scandium.[7] Apart from this phase and its isotype $ScNbN_{1-x}$,[8] only the rock-salt-type binary δ-ScN and some solid solutions of δ-ScN with binary metal nitrides[9] and the nitridoscandate $Li_3[ScN_2]$ with Sc in a very unusual tetrahedral coordination are known.[10] All this and the nitrogen-deficient disordered crystal structure of $ScTaN_{1-x}$ led us to investigate the quasi-binary system ScN–TaN, and study the crystal structure, physical properties, and

* Author to whom correspondence should be addressed. E-mail: niewa@cpfs.mpg.de. Fax: +49 (351) 4646-3002.

(1) Brokamp, Th.; Jacobs, H. *J. Alloys Compd.* **1991**, *176*, 47.
(2) Brokamp, Th.; Jacobs, H. *J. Alloys Compd*. **1992**, *183*, 325.
(3) Jacobs, H.; von Pinkowski, E. *J. Less-Common Met*. **1989**, *146*, 147.
(4) a) Brokamp, Th. Ph.D. Thesis, Universität Dortmund, Germany, 1991. (b) Balbarin, V.; VanDover, R. B.; DiSalvo, F. J. *J. Phys. Chem. Solids* **1996**, *57*, 1919.
(5) Zachwieja, U.; Jacobs, H. *Eur. J. Inorg. Solid State Chem*. **1991**, *28*, 1055.
(6) Cario, L.; Gál, Z. A.; Braun, Th. P.; DiSalvo, F. J.; Blaschkowski, B.; Meyer, H.-J. *J. Solid State Chem*. **2001**, *162*, 90.
(7) Lengauer, W.; Ettmayer, P. *J. Less-Common Met*. **1988**, *141*, 157.
(8) Lengauer, W. *J. Solid State Chem*. **1989**, *82*, 186.
(9) See, e.g.: Aivazov, M. I.; Rezchikova, T. V. *Zh. Neorg. Khim*. **1977**, *22*, 458; *Russ. J. Inorg. Chem. (Engl. Transl.)* **1977**, *22*, 250.
(10) Niewa, R.; Zherebtsov, D. A.; Leoni, S. *Chem.—Eur. J*. **2003**, *9*, 4255.

10.1021/ic040027+ CCC: $27.50
Published on Web 09/02/2004

Table 1. Selected Unit Cell Parameters of Phases δ-ScN ($Sc_{1-x}Ta_xN$), $ScTaN_2$, and ϵ-TaN ($Ta_{1-x}Sc_xN$) in Thermal Equilibrium after Annealing[a]

T (K)	δ-ScN (1) *a* (pm)	$ScTaN_2$ (2) *a*, *c* (pm)	ϵ-TaN (3) *a*, *c* (pm)	β-Ta_2N (4) *a*, *c* (pm)	phase composition
1370	449.84(5)				1
1820	446.30(5), 10% Ta				1
1820	445.94(5)	305.45(5), 1056.8(2)			1 + 2
1820		305.34(3), 1056.85(9)			2
1820			519.04(5), 290.73(5), 5% Sc		3
1870	444.44(5)	305.54(5), 1057.3(3)			1 + 2
1870		304.85(5), 1055.6(2)	518.49(5), 290.57(5)		2 + 3
1870			518.74(5), 290.60(5)		3
1970	449.75(5)				1
1970	444.17(5)			304.61(5), 493.0(1)	1 + 4

[a] Experiments are ordered by increasing annealing temperature and increasing Ta content.

bonding of the only intermediate we could identify in this system: $ScTaN_2$.

Experimental Section

Synthesis and Characterization. All manipulations were carried out under dry argon in a glovebox (content of O_2, H_2O < 0.1 ppm). All reactions were carried out in Ta crucibles.

For preparation of δ-ScN, Sc metal (Hunan Institute of Rare-Earth Metals Materials, China; sublimed, dendritic, chemical analyses: w(O) = 0.09(2)%, w(N, C) below the determination limit, ≪0.01%) was heated in a nitrogen atmosphere (Messer-Griesheim, 99.999%, additionally purified by passing over molecular sieves, Roth 3 Å, and BTS catalyst, Merck) within an induction furnace (Hüttinger TIG 5/300, W-crucible) to T = 1670 K, held at this temperature for 1 h, and cooled by switching off the current. The dark brown material was ground to a fine powder and passed through a 20 μm sieve. The resulting powder with a composition of $Sc_{1.00(1)}N_{0.98(2)}O_{0.007(2)}$ resulting from chemical analyses (w(Sc) = 76.4(7)%, w(N) = 23.3(6)%, w(O) = 0.19(6)%) is single phase according to X-ray powder diffraction. Ta_3N_5 was obtained as a fine red powder from reaction of $TaCl_5$ (Puratronic, 99.99%) with flowing ammonia (Messer-Griesheim, ultrahigh purity, 99.998%) of ambient pressure at T = 970 K for 5 h (w(N) = 11.43(9)%, w(O) = 0.72(8)%, i.e., $Ta_3N_{5.04(1)}O_{0.28(3)}$).

The single-phase sample of $ScTaN_2$ for diffraction experiments and physical properties measurements was prepared from fine powders of δ-ScN and Ta_3N_5 (molar ratio n(Sc)/n(Ta) = 1) at T = 1820 K (200 h) in flowing nitrogen of ambient pressure (purified as described above) (chemical analyses: w(Sc) = 16.1(2)%, w(Ta) = 69.2(3)%, w(N) = 11.1(1)%, w(O) = 0.5(2)%, i.e., $Sc_{0.93(1)}Ta_{1.00(3)}N_{2.07(2)}O_{0.08(3)}$. Experiments with different starting ratios n(Sc)/n(Ta) were performed at temperatures of T = 1820, 1870, and 1970 K under otherwise identical conditions. Selected results are given in Table 1. Samples heated in a nitrogen atmosphere to temperatures above 1970 K consisted exclusively of δ-ScN and β-Ta_2N. Under the same conditions ϵ-TaN was observed to decompose to β-Ta_2N.

Density Measurement. For the determination of the bulk density the volume of a known sample mass was measured in a helium gas pycnometer (AccyPyc 1330, Micromeritics):[11] ρ_{exptl} = 9.87(2) g/cm^3, ρ_{calcd} = 9.886 g/cm^3.

Crystal Structure Determination and Refinements. All samples were characterized by X-ray powder diffraction using an imaging plate Guinier camera (HUBER diffraction, Cu Kα_1 radiation, 4 × 15 min scans, 8° ≤ 2θ ≤ 100°). In each case, the sample was loaded between two polyimide foils in an aluminum cell with a rubber seal to exclude any moisture. Comparison of the powder patterns of the first and the final scans did not indicate any effect of significant hydrolysis during the measurement procedure.

Neutron diffraction data on a microcrystalline sample of $ScTaN_2$ were gathered at the E9 powder diffractometer at BERII, HMI Berlin, Germany. The sample was contained in a gastight vanadium cylinder (diameter 6 mm, length 51 mm, wall thickness 0.15 mm). The crystal structure parameters were obtained by a simultaneous refinement with both patterns. For initial positional parameters the data of $ScTaN_{1-x}$ were used.[7] Introduction of anti-site defects on the metal atom sites in the final refinement step improved the fits considerably. Figure 1 depicts the experimental diffraction patterns together with the calculated profiles and the difference curves of the observed and the simulated patterns as determined by least-squares refinements (program package FULLPROF[12]). Results of the refinements are given in Tables 2 and 3.

Thermal Analyses. DTA/TG measurements were performed on an STA 449C (Ar or N_2 atmosphere purified as described above, O_2 99.998%, thermocouple type S, NETZSCH Gerätebau, Selb, Germany). Temperature calibration was obtained using five melting standards in the temperature range of 370 K ≤ T ≤ 1470 K.

Magnetic Susceptibility. Measurements of the magnetization were carried out on a SQUID magnetometer (MPMS-XL7, Quantum Design) in magnetic fields in the range 20 Oe ≤ H ≤ 70 kOe in the temperature range of 1.8 K ≤ T ≤ 400 K using 104.4 mg of single-phase product sealed into a quartz tube under p = 400 mbar of He.

Electrical Resistivity. Electrical resistivity measurements were performed on a single-phase powder of $ScTaN_2$ in a sapphire die cell by the van der Pauw method in the temperature range of 4 K ≤ T ≤ 320 K. The contacts were made by pressing soft Pt spheres into the sample. All manipulations and measurements were carried out in an argon-filled glovebox with an integrated cryostat for temperature control.

Theoretical Details. Electronic structure calculations for $ScTaN_2$ have been performed using the scalar-relativistic LMTO-ASA method[13] as implemented in the Tight-Binding LMTO-ASA program package of Andersen et al.[14] The calculations within the atomic sphere approximation (ASA) include corrections from the neglect of the interstitial regions and the partial waves of higher order.[13] Interstitial spheres (E) had to be added to reduce overlap

(11) Webb P. A.; Orr, C. *Analytical Methods in Fine Particle Technology*; Micromeritics Intruments Corp.: Norcross, GA, 1997.

(12) (a) Roisnel, T.; Rodriguez-Carvajal, J. *WinPLOTR, version May 2000*, Materials Science Forum, Proceedings of the 7th European Powder Diffraction Conference, Barcelona, Spain, Trans Tech Publications Ltd.: Uetikon, Switzerland, 2000; p 188. (b) Rodriguez-Carvajal, J. *FULLPROF.2k*, version 1.6; Laboratoire Léon Brillouin: Gif-sur-Yvette, France, 2000. *Abstract of Satellite Meeting on Powder Diffraction*; Congress of the International Union of Crystallography: Toulouse, France, 1990; p 127.

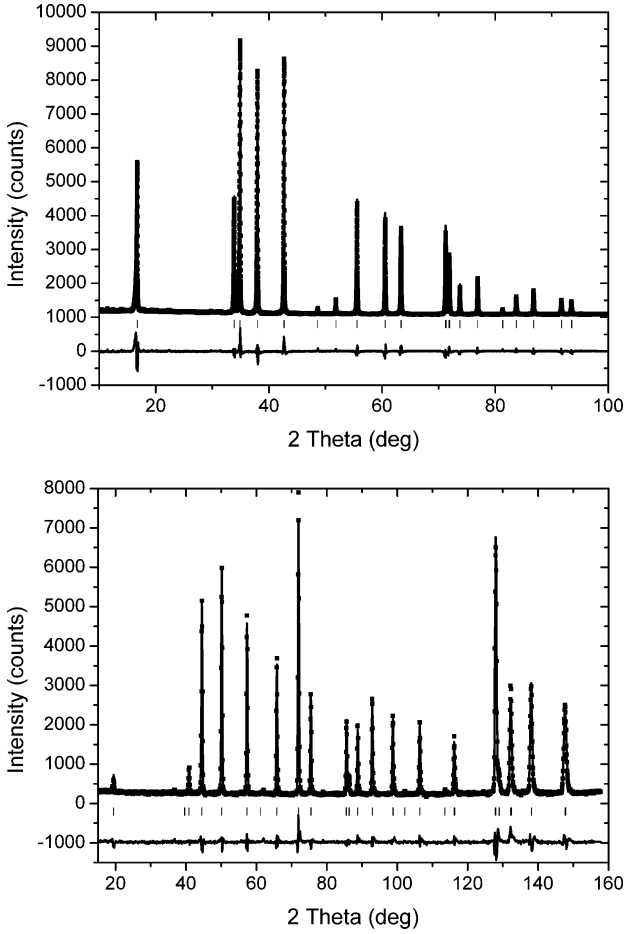

Figure 1. (a, top) X-ray (Cu Kα_1 radiation) and (b, bottom) neutron (λ = 179.609(4) pm) powder diffraction diagram of $ScTaN_2$. The measured data are plotted as points, the continuous line represents the calculated profile, and the lower line shows the difference between the calculated and observed intensities. The marks below the data indicate the positions of the reflections.

Table 2. Profile Refinement Parameters for $ScTaN_2$

	X-ray data	neutron data
space group, *Z*	$P6_3/mmc$, No. 194, 2	
a (pm), Guinier	305.34(3)	
c (pm)	1056.85(9)	
V (10^6 pm^3)	85.33	
a (pm), Rietveld	305.343(6)	
c (pm)	1056.42(1)	
wavelength (pm)	Cu Kα_1	179.609(4)[a]
2θ range (deg)	10−98	14−156
step size (deg)	0.005	0.078
no. of params refined	33	
no. of structural params	8	
χ^2	1.55	0.94
reliability values R_{Bragg}/R_f	0.061/0.047	0.042/0.032

[a] Allowed to vary in the refinement.

Table 3. Positional and Isotropic Displacement Parameters for $ScTaN_2$

atom	site	x	y	z	occ	*B* (10^{-4} pm^2)
Sc/Ta	2a	0	0	0	0.926(5)/0.074	0.67(4)
Ta/Sc	2d	1/3	2/3	3/4	0.97(1)/0.03	0.28(3)
N	4f	1/3	2/3	0.1231(2)	1	0.31(4)

of the atomic spheres. Radii used were *r*(Sc) = 148.6 pm, *r*(Ta) = 146.0 pm, *r*(N) = 105.4 pm, *r*(E1) = 72.3 pm, and *r*(E2) = 71.1 pm. The basis set consisted of the Sc(4s,4p,3d), Ta(6s,6p,5d), N(2s,2p,3d), and E(1s,2p) LMTOs; Sc(4p), N(3d), and E(2p) were downfolded.[15]

Crystal orbital Hamiltonian populations (COHPs) were calculated according to the literature[16] with a special module implemented into the TB-LMTO-ASA program package.[17] The basis set was slightly modified compared to the standard LMTO calculation: as recommended,[17] the empty orbitals were not explicitly included but all downfolded.

Within the TB-LMTO-ASA code a three-dimensional map $\eta(r)$ of the electron localization function (ELF)[18] was evaluated using all orbitals (i.e., core and valence orbitals) of the converged solution. In the density functional approach, this real-space quantity depends on the local excess of kinetic energy density due to the Pauli principle (Pauli kinetic energy density) relative to a uniform distribution.[19] Applying the topological procedure proposed by Bader for the electron density,[20] the whole field $\eta(r)$ can be divided into the basins of core attractors, bonding attractors, and nonbonding attractors. Topological analysis of $\eta(r)$ was performed with the program system TopAn.[21] Further information on the calculation, interpretation, and application is given in the literature.[22,23]

Results and Discussion

$ScTaN_2$ was obtained by high-temperature treatment of mixed fine powders of δ-ScN and Ta_3N_5 or ϵ-TaN, respectively; the latter phase formed from in situ thermal decomposition of the binary tantalum(V) nitride. No indications for a nitrogen-deficient phase could be found, but the unit cell parameters refined for $ScTaN_2$ are nearly identical to those reported for $ScTaN_{1-x}$.[7] The solid solubility of ScN in the hexagonal ϵ-TaN[24] appears to be small within the stability region of this phase up to T = 2000 K in a N_2 atmosphere. Above this temperature ϵ-TaN decomposes to form β-Ta_2N[25] under the applied conditions, and at approximately the same temperature, $ScTaN_2$ decomposes into δ-ScN ($Sc_{1-x}Ta_xN$), β-Ta_2N, and N_2. In an argon atmosphere this decomposition already starts at about T = 1250 K. Combined thermogravimetric and differential thermal analyses (TG/DTA) on $ScTaN_2$ in a nitrogen atmosphere did not reveal any phase transition or significant weight change up to T = 1850 K. TG/DTA in an oxygen atmosphere (Figure 2) shows only a

(13) Andersen, O. K. *Phys. Rev. B* **1975**, *12*, 3060.
(14) Jepsen, O.; Burkhardt, A.; Andersen, O. K. *The program TB-LMTO-ASA*, version 4.7; Max-Planck-Institut für Festkörperforschung: Stuttgart, Germany, 1999.
(15) Lamprecht, W. R. L.; Andersen, O. K. *Phys. Rev. B* **1986**, *34*, 2439.
(16) Dronskowski, R.; Blöchl, P. E. *J. Phys. Chem.* **1993**, *97*, 8617.
(17) Boucher, F.; Jepsen, O.; Andersen, O. K. *Supplement to the TB-LMTO-ASA V 4.7 program*; Max-Planck-Institut für Festkörperforschung: Stuttgart, Germany, 1996.
(18) Becke, A. D.; Edgecombe, K. E. *J. Chem. Phys.* **1990**, *92*, 5397.
(19) Savin, A.; Jepsen, O.; Flad, H. J.; Andersen, O. K.; Preuss, H.; von Schnering, H. G. *Angew. Chem., Int. Ed. Engl.* **1992**, *31*, 187.
(20) Bader, R. F. W. *Atoms in Molecules: A Quantum Theory*; Oxford University Press: Oxford, 1990.
(21) Wagner, F. R. *Program system TopAn for topological analysis of scalar 3d fields*, V5.2; Max-Planck-Insitut für Chemische Physik fester Stoffe: Dresden, Germany, 2003.
(22) Savin, A.; Nesper, R.; Wengert, S.; Fässler, T. F. *Angew. Chem., Int. Ed. Engl.* **1997**, *36*, 1808.
(23) Wagner, F. R.; Kohout, M. Scientific ELF Homepage. http://www.cpfs.mpg.de/ ELF.
(24) (a) Brauer, G.; Zapp, K. H. *Z. Anorg. Allg. Chem.* **1954**, *277*, 129. (b) Brauer, G.; Killian, W. *Z. Anorg. Allg. Chem.* **1979**, *452*, 17.
(25) Conroy, L. E.; Nørlund Christensen, A. *J. Solid State Chem.* **1977**, *20*, 205.

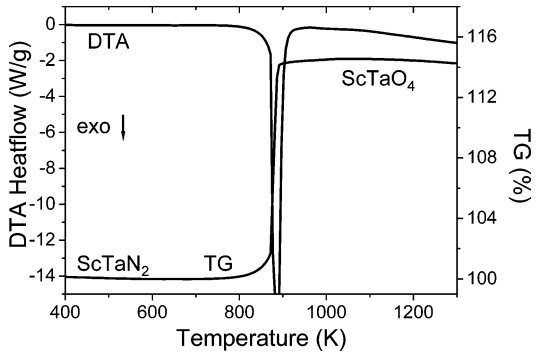

Figure 2. TG/DTA diagram of the reaction of $ScTaN_2$ with O_2 (heating rate 10 K/min).

slight weight increase up to about $T = 800$ K. Above this temperature oxidation accelerates, leading to a weight increase of $\Delta m/m = 0.141$, consistent with the formation of $ScTaO_4$, as observed in the subsequent powder X-ray diffraction patterns (wolframite structure type).[26] This step in the TG curve is accompanied by a strongly exothermic signal in the DTA curve with $T_{onset} = 873$ K, a considerably lower temperature compared with the oxidation temperature of δ-ScN under these conditions ($T_{onset} \approx 970$ K).

In combination with small amounts of rare-earth metals a stabilization of the high-temperature rock-salt-type δ-TaN to lower temperatures was reported,[8] but for Sc we did not observe the formation of this cubic phase. On the other hand, the homogeneity range between cubic δ-ScN (rock-salt-type crystal structure) and $Sc_{1-x}Ta_xN$ is quite considerable (≥ 10 mol % at 1820 K). The unit cell parameters of the solid solutions in thermal equilibrium with $ScTaN_2$ decrease with increasing temperature, due to increasing solubility for Ta from $a = 449.84(5)$ pm for δ-ScN ($x = 0$) to $a = 446.30(5)$ pm for $x = 0.10$ (see Table 1). Compared to the unit cell parameter of cubic δ-TaN of $a = 436$ pm,[27] this steep decrease of the volume with x means a negative deviation from Vegard's law and, thus, already indicates the formation of the ternary phase $ScTaN_2$.

$ScTaN_2$ crystallizes hexagonally in the space group $P6_3/mmc$. The crystal structure can be described from the viewpoint of close-packed metal atoms in an ordered $(hc)_2$ layered arrangement (Jagodzinski−Wyckoff notation) with occupation of pairs of face-sharing octahedra Ta_3Sc_3 by N^{3-}, which in turn share edges. Perhaps preferably, the crystal structure may be described as stacking of close-packed layers of the large N^{3-} species with the metal atoms in octahedral (Sc) and trigonal prismatic (Ta) voids. In the latter description stacking along the c-axis takes place with the sequence ...AbAγBaBγ... (A and B denote close-packed layers of N, a and b denote Ta, and γ denotes Sc). As in the cubic δ-ScN and hexagonal ϑ-TaN (WC structure type)[24,28] the metal atoms are coordinated octahedrally and trigonally prismatically, respectively. Thus, the formation of the crystal structure of $ScTaN_2$ can be described as an intergrowth structure of

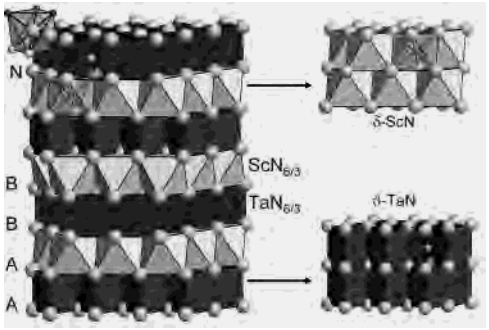

Figure 3. Part of the crystal structure of $ScTaN_2$ with alternating layers of edge-sharing trigonal $TaN_{6/3}$ prisms and edge-sharing $ScN_{6/3}$ octahedra. For comparison sections of the crystal structures of δ-ScN and ϑ-TaN are depicted on the right side.

alternating slabs of these two binaries.[29] This fact is illustrated in Figure 3. The small homogeneity region observed corresponds to a small degree of anti-site defects as has been concluded from the joint refinement of X-ray and neutron diffraction patterns (see Table 3). Chemical analyses and the refinement of the powder pattern lead to atomic ratios n(Sc)/n(Ta) of 0.93(1) and 0.92(1), respectively. The excess of Ta might be explained by the use of Ta crucibles during preparation. A similar formation of anti-site defects up to a level of about 15% was observed for, e. g., $LiMoN_2$.[30] The crystal structure of $ScTaN_2$ shows an interesting relation to that of $Ta_5N_6 \equiv (Ta_2\square)^{oc}(Ta_3)^{tp}N_6$ ($\square$ denotes a vacancy on an octahedral site, the superscript oc means octahedrally coordinated, and the superscript tp means trigonally prismatically coordinated),[31,32] representing a defect variant with ordered vacancy positions at the octahedral voids. A similar correlation can be seen with $Li_{1-x}Ta_{3+x}N_4$ (with $x = 0$, $LiTa_3N_4$) and $Mg_{1-x}Ta_{2+x}N_3$ (with $x = 0$, $MgTa_2N_3$),[2] which can be related to $(Li_{1/2}{}^{+}Ta_{1/2}{}^{5+})^{oc}(Ta^{3+})^{tp}N_2$ and $(Mg_{2/3}{}^{2+}$-$Ta_{1/3}{}^{5+})^{oc}(Ta^{3+})^{tp}N_2$, respectively.

The atomic arrangement of $Sc^{oc}Ta^{tp}N_2$ is identical to the arrangements in, e.g., $Ba^{tp}Ce^{oc}N_2$,[33] β-$Rb^{tp}Sc^{oc}O_2$,[34] $Li^{oc}Nb^{tp}O_2$,[35] and β-$Sc^{oc}Cr^{tp}C_2$.[36] While for $Nb^{3+}(4d^2)$ the formation of trigonal prismatic coordination may be reasoned as discussed below, large Ba^{2+} and Rb^{+} ions are often found to prefer trigonal prismatic coordination in contrast to the smaller ions of groups 1 and 2 of the PSE. The crystal structures under consideration can be compared using two parameters, the c/a ratio and the z-parameter of the Wyckoff position 4f (elements N, O, and C). The crystal structure of the acetylide is restricted by the formation of C_2 ions and,

(26) Rooksby, H. P.; White, E. A. D. *Acta Crystallogr.* **1963**, *16*, 888.
(27) Gatterer, J.; Dufek, G.; Ettmayer, P.; Kieffer, R. *Acta Crystallogr., A* **1975**, *31*, 99.
(28) Gatterer, J.; Dufek, G.; Ettmayer, P.; Kieffer, R. *Monatsh. Chem.* **1975**, *106*, 1137.
(29) Parthé, E. *Elements of Inorganic Structural Chemistry*; Pöge: Leipzig, Germany, 1990.
(30) Elder, S. H.; Doerrer, L. A.; DiSalvo, F. J.; Parise, J. B.; Guyomard, D.; Tarascon, J. M. *Chem. Mater.* **1992**, *4*, 928.
(31) Fontbonne, A.; Gilles, J. C. *Rev. Int. Hautes Temp. Refract.* **1969**, *6*, 181.
(32) (a) Gilles, J.-C. *C. R. Acad. Sci.* **1968**, *166*, 546. (b) Vendl, A. *Monatsh. Chem.* **1978**, *109*, 1009.
(33) Seeger, O.; Strähle, J. *Z. Naturforsch.* **1994**, *49b*, 1169.
(34) Wiench, H.; Brachtel, G.; Hoppe, R. *Z. Anorg. Allg. Chem.* **1977**, *436*, 169.
(35) Meyer, G.; Hoppe, R. *J. Less-Common Met.* **1976**, *46*, 55.
(36) Pöttgen, R.; Witte, A. M.; Jeitschko, W.; Ebel, T. *J. Solid State Chem.* **1995**, *119*, 324.

Table 4. Selected Distances (pm) and Angles (deg) in $ScTaN_2$

Sc−N	219.1(1)	×6	N−Sc−N	88.36(4)	91.64(9)	180
Ta−N	221.5(1)	×6	N−Ta−N	74.50(9)	87.16(4)	133.09(9)

thus, by comparably short distances d(C−C). This leads to different relations of compressed trigonal $CrC_{6/2}$-prisms and elongated $ScC_{6/3}$-octahedra in β-$ScCrC_2$ ($z = 0.1627$, $c/a = 2.83$), while in $BaCeN_2$, as the other extreme, the trigonal $BaN_{6/3}$-prisms are elongated along [001] and the $CeN_{6/3}$-octahedra are somewhat compressed ($z = 0.097$). Interestingly, compounds such as $Cr_2Al^{tp}C^{oc}$ ($Cr_4Al_2C_2$) and $V_2P^{tp}C^{oc}$ crystallize in an anti-type arrangement of this crystal structure with small parameters $z < 0.1$ ($c/a = 4.48$, 3.55, respectively)[37,38] and, thus, elongated trigonal prisms. It is also noteworthy that $ScTaO_4$, the reaction product of $ScTaN_2$ with O_2, can also be described in terms of alternating layers of polyhedra ScO_6 and $Ta^{+5}O_6$ (condensed to infinite chains), but both metal atoms are in octahedral coordination (wolframite structure type).[26]

The structural arrangement of $ScTaN_2$ avoids face-sharing of coordination polyhedra of the metal atoms. Similar layered crystal structures are known from ternary transition-metal molybdenum/tungsten nitrides, e.g., $FeWN_2$[39] with tungsten in trigonal prisms, but typically face-sharing polyhedra, or $MnMoN_2$ and β-$MnWN_2$[39,40] with structural models proposed to be basically identical with that of $ScTaN_2$. The structural relationships between different arrangements of layers of edge-sharing octahedra alternating with various layers of different kinds are directly evident: the additional layers comprise edge-sharing trigonal prisms in the β-$RbScO_2$ structure type ($ScTaN_2$), edge-sharing octahedra in the α-$NaFeO_2$ structure type ($Na[TaN_2]$, $Ca[TaN_2]$),[3,4] and linearly coordinated ions in the delafossite structure type ($Cu[TaN_2]$).[5]

Distances d(Sc−N) = 219.1(1) pm and d(Ta−N) = 221.5(1) pm in $ScTaN_2$ are similar to those in δ-ScN with d(Sc−N) = 225.6 pm[41] and ϑ-TaN with d(Ta−N) = 222.6 pm;[24,28] interestingly, the distance relation is reversed (see Table 4). The $TaN_{6/3}$ layer is somewhat expanded, leading to slightly longer distances d(Ta−Ta) = 305.34(3) pm compared to those in ϑ-TaN (d(Ta−Ta) = 293.1 pm). The reason is found in the match with the $ScN_{6/3}$ layers: The distance d(Sc−Sc) = 305.34(3) pm is compressed compared to the corresponding distance in δ-ScN (d(Sc−Sc) = 314.0 pm). The distance d(N−N) = 268.1(3) pm within the trigonal prisms along the c-axis is comparably short for N in close-packed arrangements, but significantly larger than the shortest distance d(N−N) = 256 pm known so far within a trigonal prism coordinating Mo^{5+} in $LiMoN_2$.[30] Noteworthy is a comparison of the volumes of the different polyhedra in $ScTaN_2$ and the relevant binary phases: the trigonal prism TaN_6 has a volume of 10.83×10^6 pm^3 in $ScTaN_2$ nearly identical to 10.77×10^6 pm^3 in ϑ-TaN, while the volume of the octahedron ScN_6 with 14.01×10^6 pm^3 is significantly smaller than 15.17×10^6 pm^3 in δ-ScN. This finding may result from the anti-sites' disorder as well as the higher Ta content compared with the ideal composition.

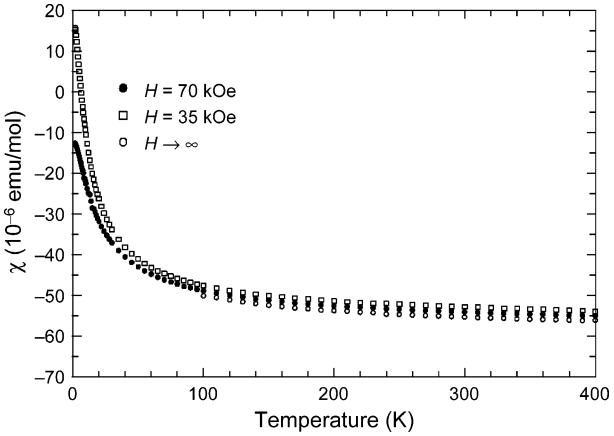

Figure 4. Magnetic susceptibility of $ScTaN_2$ at different fields as a function of temperature. Minor ferromagnetic impurities ($T_C > 400$ K) were eliminated by extrapolation of $\chi(H)$ to $1/H \rightarrow \infty$ using the two measurements at high fields.

The magnetic susceptibility $\chi = M/H$ of $ScTaN_2$ for high magnetic fields is displayed in Figure 4. For $T > 100$ K the susceptibility is only weakly temperature and field dependent. The upturn of $\chi(T)$ toward low T is due to minor paramagnetic impurities (corresponding to a molar fraction of $S = 1/2$ species of $x_P = 0.0023$). The weak dependence on the external magnetic field is explained by traces of ferromagnetic impurities with $T_C > 400$ K (corresponding to a mass fraction of Fe metal $m_{Fe}/m < 2 \times 10^{-6}$). Extrapolation of $\chi(T, H)$ for $1/H \rightarrow 0$ yields corrected values for $T > 100$ K. At $T = 300$ K the corrected susceptibility is $\chi = -55(5) \times 10^{-6}$ emu/mol, roughly consistent with the sum of the diamagnetic increments[42] of $(-6 - 14 - 2 \times 12) \times 10^{-6}$ emu/mol, where for N^{3-} a value of -12×10^{-6} emu/mol has been adopted from the value for O^{2-}.

The electrical resistivity $\rho(T)$ (see Figure 5) of $ScTaN_2$ is large (on the order of 10^{-2} Ω cm) and increases strongly with increasing temperature. Therefore, $ScTaN_2$ may represent a semimetal, or despite the observed temperature dependence, from the order of magnitude of $\rho(T)$, $ScTaN_2$ can be classified to represent a semiconductor with a small gap and a strong contribution from defects giving some electrical conductivity. Both interpretations are consistent with the results of the electronic structure calculation, the level of anti-site defects observed in the crystal structure refinement, and the homogeneity range of the phase.

The calculated total DOS for the valence electrons consists of three separate groups of structures (Figure 6): at the bottom of the valence bands (at about [−17.5 eV, −14.5 eV], relative to E_F) the majority of N(2s) states are found

(37) Jeitschko, W.; Nowotny, H.; Benesovsky, F. *Monatsh. Chem.* **1963**, *94*, 672.
(38) Boller, H.; Nowotny, H. *Monatsh. Chem.* **1968**, *99*, 672.
(39) Bem, D. S.; Lampe-Önnerud, C. M.; Olsen, H. P.; zur Loye, H.-C. *Inorg. Chem.* **1996**, *35*, 581.
(40) Houmes, J. D.; Bem, D. S.; zur Loye, H.-C. In *Covalent Ceramics II: Non-Oxides*, MRS Symposium Proceeding, Boston, MA, 1993; Barron, A. R., Fischman, G. S., Fury, M. A., Hepp, A. F., Eds.; MRS: Pittsburgh, Pennsylvania, Vol. 327, p 153.
(41) a) Friederich, E.; Sittig, L. *Z. Anorg. Allg. Chem.* **1925**, *143*, 293. (b) Niewa, R.; Zherebtsov, D. A.; Kirchner, M.; Schmidt, M. Manuscript in preparation.
(42) *Landolt-Börnstein*; Springer: Berlin, 1984; Neue Serie, Band 12, Suppl. 4a.

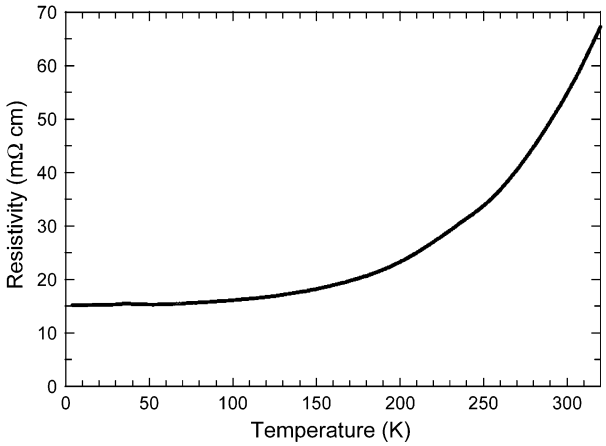

Figure 5. Electrical resistivity of $ScTaN_2$ as a function of temperature. A typical geometry factor error is a factor of 2.

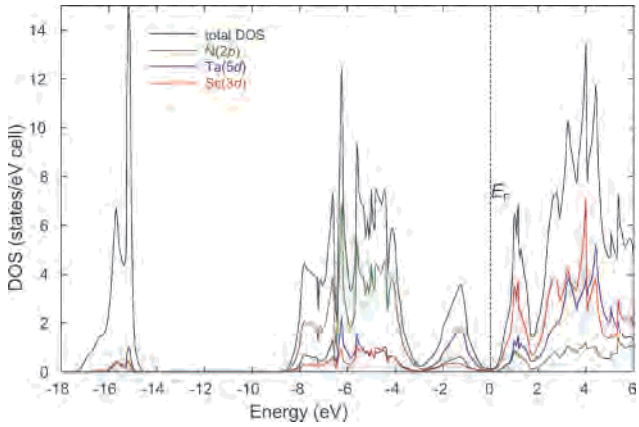

Figure 6. Total DOS and DOS projections for $ScTaN_2$.

(feature A). The broad feature at [−8.5 eV, −3 eV] can be attributed to the majority of N(2p) states with covalent mixing of Sc(3d) and Ta(5d) (feature B). The DOS feature at [−3 eV, E_F] consists of Ta(5d) states with admixtures of N(2p) states (feature C). In our calculations no true band gap but a pseudogap occurs with some states remaining at E_F, indicating a semimetallic state. As the LDA is known to give too small band gaps, we could accept that the compound is a semiconductor in reality, consistent with the physical property measurement results discussed above.

The bonding picture emerging from DOS projections is corroborated by COHP calculations (Figure 7): COHP(Sc−N) gives the typical behavior for partially covalent/ionic interactions between a closed shell (formally N^{3-}) nitride species and a formally Sc^{3+} species. All the available bonding states (coinciding with DOS feature B) are filled, and the corresponding antibonding ones just start above E_F. COHP-(Ta−N) behaves similarly in the energy region of DOS feature B, but in DOS region C Ta(5d)−N(2p) antibonding interactions occur. This behavior is generally expected for formal d^2-Ta^{3+}−N^{3-} interactions since the remaining Ta-(5d) electrons must lead to such contributions. Because Ta has available itinerant d electrons, it can be expected that these do not form only antibonding interactions, and indeed, significant Ta−Ta bonding interactions occur within each Ta plane. In fact, this is a situation very similar to that of

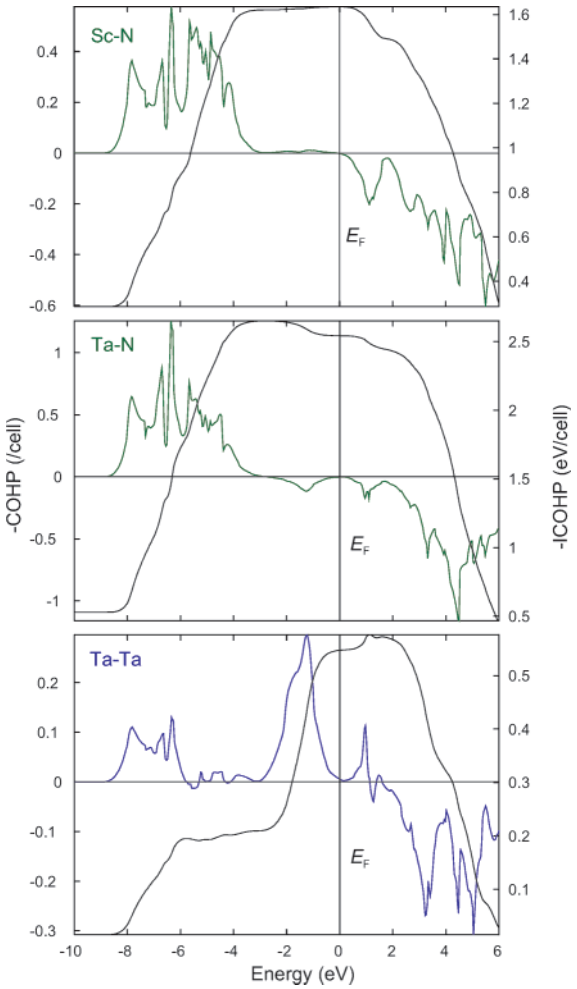

Figure 7. COHP(E) and ICOHP(E) diagrams for selected interactions Sc−N (top), Ta−N (middle), and Ta−Ta (bottom) in $ScTaN_2$.

binary ϑ-TaN, where the distance d(Ta−Ta) = 294 pm is shorter than d(Ta−Ta) = 305 pm in $ScTaN_2$.

The spatial organization of the metal−metal bond was studied using the real space quantity ELF. As can be seen in Figure 8, the topology of the $\eta(r)$ field for $ScTaN_2$ shows a significant trigonal structuring of the outer core shell (i.e., fifth shell) of Ta whose three in-plane attractors point in the direction of the three "empty" neighboring trigonal prisms. In the valence region, at the center of each empty trigonal prism ELF displays an attractor (η = 0.63), which forms a trisynaptic basin (i.e., it is directly attached to three Ta cores). The specific arrangement of the trisynaptic basins and the consistent orientation of the significant structuring of the Ta fifth atomic shell indicates a direct participation of Ta fifth shell electrons[43] in Ta−Ta bonding. Thus, the seemingly empty trigonal prisms are in fact the place of those important Ta−Ta interactions. Each Ta atom has six equidistant homoatomic neighbors (d(Ta−Ta) = 305 pm) within (001). Instead of six two-center bonds per Ta atom, ELF points to the formation of three three-center bonds per Ta. Interestingly, we find the same behavior of ELF for several other compounds with a similar partial structure and a formal d^2

(43) Kohout, M.; Wagner, F. R.; Grin, Yu. *Theor. Chem. Acc.* **2002**, *108*, 150.

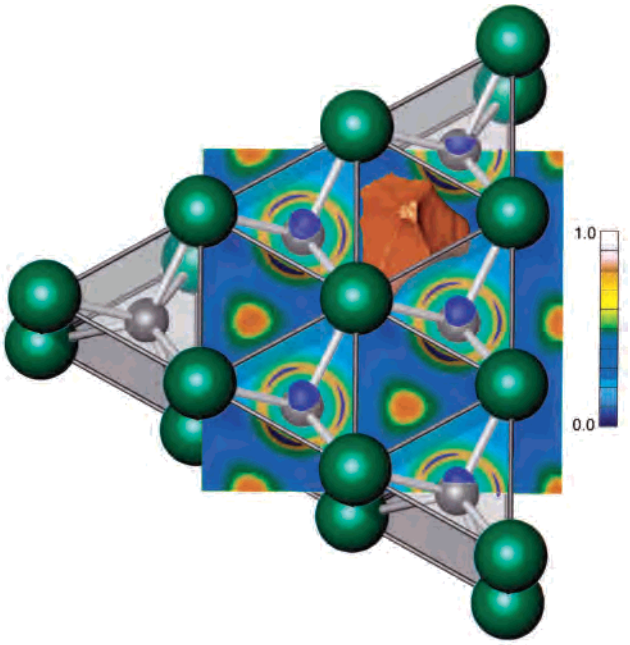

Figure 8. ELF isosurface for $ScTaN_2$: gray spheres, Ta; green spheres, N. Blue localization domains of ELF ($\eta = 0.588$) display trigonal structuring of the fifth Ta atomic shell according to the spatial organization of the trisynaptic Ta−Ta bonding basins (one of which is shown in brown). The corresponding attractors of ELF are located at the center of the empty trigonal prisms of this substructure of $ScTaN_2$.

configuration of the transition metal: from LDA band structure calculations WC and ϑ-TaN are both semimetals (for WC this has been corroborated by de Haas−van Alphen measurements);[44] however, they are predicted to possess a qualitatively different Fermi surface.[45] While ϑ-TaN exhibits only bands which are crossing the Fermi level in connection with dispersion perpendicular to the hexagonal plane, for WC bands with dispersion within the plane and crossing E_F are present. Moreover, MoS_2 is even a semiconductor and shows the same metal−metal three-center bonding pattern in ELF as WC, ϑ-TaN, and $ScTaN_2$. Thus, we found a robust bonding feature characteristic for these compounds, irrespective of the detailed electronic situation close to E_F and the corresponding electronic conductivity.

In summery, we have obtained a new ternary layered nitride with in-plane Ta−Ta three-center bonding interactions governing the crystal structure. As nitrides generally show smaller band gaps compared to, e.g., oxides, despite an ionic description of $Sc^{3+}Ta^{3+}(N^{3-})_2$, a clear distinction between semimetallic and semiconducting behavior is not possible, neither experimentally nor by electronic structure calculations. Detailed investigations in related ternary rare-earth-metal−transition-metal−nitride systems are forthcoming to gain deeper insight.

Acknowledgment. We thank Steffen Hückmann for the collection of the X-ray diffraction data, Ulrike Schmidt and Britta Bayer for performing the chemical analyses, Dr. Ulrich Burkhardt for the density measurements, and Prof. Dr. Rüdiger Kniep for his constant support and interest. The neutron diffraction data collection by Dr. Gudrun Auffermann at the E9 diffractometer operated by Dr. Daniel Többens is grateful acknowledged.

Supporting Information Available: Rietfeld refinement data for X-ray and neutron diffraction patterns of $ScTaN_2$ (PDF). This material is available free of charge via the Internet at http://pubs.acs.org.

IC040027+

(44) Ishizawa, Y.; Tanaka, T. *Solid State Commun.* **1984**, *51*, 743.
(45) Litinsky, L. B. *Solid State Commun.* **1990**, *75*, 1009.